DFT and TD–DFT investigation of IR and UV spectra of solvated molecules: Comparison of two SCRF continuum models

ARTICLE *in* INTERNATIONAL JOURNAL OF QUANTUM CHEMISTRY · MARCH 2007

Impact Factor: 1.43 · DOI: 10.1002/qua.21182

5 AUTHORS, INCLUDING:

Pierre-François Loos
Australian National University
50 PUBLICATIONS **553** CITATIONS
SEE PROFILE

Xavier Assfeld
University of Lorraine
107 PUBLICATIONS **1,661** CITATIONS
SEE PROFILE

Denis Jacquemin
University of Nantes
356 PUBLICATIONS **8,231** CITATIONS
SEE PROFILE

Eric A Perpète
University of Namur
173 PUBLICATIONS **5,996** CITATIONS
SEE PROFILE

DFT and TD-DFT Investigation of IR and UV Spectra of Solvated Molecules: Comparison of Two SCRF Continuum Models

JULIEN PREAT,[1] PIERRE-FRANÇOIS LOOS,[2] XAVIER ASSFELD,[2] DENIS JACQUEMIN,[1] ERIC A. PERPÈTE[1]

[1]*Laboratoire de Chimie Théorique Appliquée, Facultés Universitaires Notre-Dame de la Paix, Rue de Bruxelles, 61, 5000 Namur, Belgium*

[2]*Equipe de Chimie et Biochimie Théoriques, UMR CNRS-UHP 7565, Université Henri Poincaré Nancy 1-BP 239, 54506 Vandoeuvre-lès-Nancy Cedex-France*

Received 28 April 2006; accepted 15 June 2006
Published online 3 October 2006 in Wiley InterScience (www.interscience.wiley.com).
DOI 10.1002/qua.21182

ABSTRACT: We report the calculation of liquid-phase infrared (IR) and ultraviolet (UV) spectra in the framework of the solute's response to the reaction field of several solvents. In particular, we compare these two properties for the multipolar expansion model developed in the Nancy continuum model (NCM) and the polarized continuum model (PCM) scheme developed in Pise and Naples. All calculations are carried out at the (TD-)DFT/6-311G(2*d*,2*p*) level of theory. The cavity size used for modeling the solute effects on the IR and UV spectra are examined. To calibrate the solute cavity size, we have investigated the IR spectra of coumarin and of a set of 14 additional solutes of different size and polarity in several dielectrical surroundings. It turns out that: (i) PCM and NCM present an identical behavior when a common cavity is used to calibrate the models; and (ii) for both NCM and PCM models, the IR spectra are highly sensitive to the solute and solvent polarity. The UV/VIS investigation of coumarin derivatives

Correspondence to: J. Preat; e-mail: julien.preat@fundp.ac.be

This article contains supplementary material available via the Internet at http://www.interscience.wiley.com/jpages/0020-7608/suppmat/.

Contract grant sponsor: FRIA.
Contract grant sponsor: FNRS–FRFC.
Contract grant sponsor: Loterie Nationale.
Contract grant number: 2.4578.02.
Contract grant sponsor: FUNDP.
Contract grant sponsor: CGRI.

demonstrates that both models provide close estimates of λ_{max} independent of the solute cavity size. Int J Quantum Chem 107: 574–585, 2007

Key words: coumarin; density functional theory; IR spectra; electronic spectra; solvent effects; PCM; NCM; SCRF

1. Introduction

Solvent effects on the thermodynamics and kinetics of chemical and biological phenomena are the object of a continued interest. In general, the aim is to describe chemical processes in solution by using theoretical methods modeling solvent effects, at a level of accuracy comparable to that attainable for isolated solute molecules. In this scope, computational methods have proved to be very powerful tools for understanding solute–solvent interactions and predicting structures, spectra, as well as reactivity in condensed phase [1]. Modeling the solvent by means of a continuum is particularly attractive, owing to its reduced computational costs with respect to methods explicitly representing the surrounding solvent. In a continuum model, based on the self-consistent reaction field (SCRF) principle, the ensemble average of solute–solvent interactions at thermal equilibrium is directly calculated [2, 3]. This approximation is valid if no specific interactions exist between the solute and the solvent (e.g., as H bonds).

This work aims to report a comparison of two different SCRF formalisms: the multipolar expansion method [Nancy continuum model (NCM)] developed by Rivail and Rinaldi and the polarizable continuum model (PCM) of Miertus, Scrocco, and Tomasi [2, 3]. In this study, we compare the infrared (IR) and ultraviolet (UV) spectra of molecules containing prototypical polar groups, that we calculate in different dielectric surroundings with both solvation models. In general, when small solutes are treated quantum mechanically, the cost of a SCRF calculation that includes solvent effects is identical for each model and is not much greater than that of the corresponding gas-phase calculation. The test molecules used in this study derive from coumarin (Fig. 1). Natural or synthetic coumarin derivatives are widely used for their biologic, medical, and physicochemical applications. Indeed, they exhibit huge physiological properties (which are biocompatible, with some of them showing anticancer, anticoagulant activities) [4]. Moreover, a large part of the coumarin derivatives constitutes a class of dyes that are widely applied, especially as laser dyes. These dyes own their success in this domain to their high emission properties, their high chemical stability, and to their relatively easy synthesis.

This study is organized as follows: Section 2 deals with the methodology and compares the two SCRF models (cavity building, electrostatic and nonelectrostatic interactions calculation). Section 3 gathers the comparison of the spectroscopic results obtained with both models. Section 3.1 presents the IR spectra and determines the conditions under which the SCRF models can be calibrated to experiment. In Section 3.2, we analyze the maximum absorption wavelength of UV/time-dependent-density functional theory (TD-DFT) spectra of a set of five substituted coumarins. To our knowledge, this work presents the first TD-DFT calculations performed within the NCM formalism.

2. Methodology

The PCM [5–12] is one of the most widely used approaches for evaluating bulk solvent effects. In PCM, one divides the problem into a solute part (the coumarin dye) lying inside a cavity, and a solvent part represented as a structureless material, characterized by its dielectric constant as well as other parameters, such as molar volume and polarizability. In this model, the solute charge distribution is represented as a continuous electron density, associated with a fixed nuclear configuration inside the solute cavity, and the solvent reaction field is expressed in terms of a set of charges distributed all over the solute cavity surface. These charges are induced by the solute charges distribution, thus

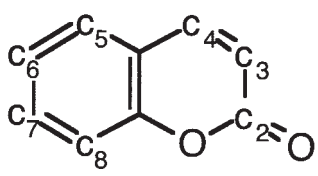

FIGURE 1. Sketch of coumarin structure and numbering of the substitution positions.

expressing the mutual solute–solvent polarization. In PCM, the surface charges are obtained by numerically solving the Poisson equation with the integral equation formalism (IEF) code [7, 10–12]. The calculation of these charges authorizes the determination of electrostatic contribution to the solvation energy. The ensemble treatment of the nonelectrostatic contributions, including the dispersive (based on the McWeeny theory formulation [12] using dynamic polarizabilities) and the cavitation [13–15] terms, is carried out using empiric relations. It is important to underline that only the electrostatic term is needed to get the wave function of the solute (nonelectrostatic contributions are considered as a corrective post-treatment of the model). In NCM formalism [16–21], the Coulomb solute–solvent interactions energy is evaluated via a multicentric multipolar Taylor expansion of the electrostatic potential. This potential is called reaction potential, giving rise to a reaction field. The first derivative of the electrostatic potential, $R_l^m(I)$, is proportional to the reaction field factors $f_{ll'}^{mm'}(I, J)$ and the multipole of rang l' evaluated at a center J, $M_{l'}^{m'}(J)$ according to the following equation:

$$R_l^m(I) = \sum_J \sum_{l'} \sum_{m'} f_{ll'}^{mm'}(I, J)\, M_{l'}^{m'}(J), \qquad (1)$$

where $f_{ll'}^{mm'}(I, J)$ depends only on the cavity shape and on the relative dielectric constant of the solvent. It is computed numerically by using the continuity condition of the electrostatic potential at a large enough point of the surface. In this study, we use the Gaussian averaged distribution (GAD) to represent the charge distribution with the multicentric multipole distribution [22]. Following the theory of Vigne-Maeder and Claverie [23], the multipole of rank l calculated at a center O, $\mathbf{M}_l(O)$, can be evaluated by means of a distribution on the N atomic centers I:

$$\sum_I w(OI)\mathbf{T}_{OI}\mathbf{M}_l(O), \qquad (2)$$

where $\mathbf{T}_{OI}$ is a translation operator from O to I, and $w(OI)$ is a Gaussian weight of the multipole calculated at a center O and translated to center I:

$$w(OI) = \frac{1}{N}\frac{e^{-JI^2}}{\sum_{K=1}^{N} e^{-JK^2}}. \qquad (3)$$

In this context, the Hartree–Fock or Kohn–Sham matrix element takes the form:

$$F_{\mu\nu} = F^{\circ}_{\mu\nu} + \sum_I \sum_J \sum_l \sum_{l'} \sum_{m'} M_{l'}^{m'}(J)\, f_{ll'}^{mm'}(J, I)\, \langle\mu|\mathbf{M}_l^m|\nu\rangle_l, \qquad (4)$$

where $M_{l'}^{m'}(J)$ is a component of the distribution on center J, and $\langle\mu|\mathbf{M}_l^m|\nu\rangle_l$ is a (μ, ν) component of the matrix associated with the M_l^m component on center I, which is given, in the GAD formalism, by the equation:

$$\langle\mu|\mathbf{M}_l^m|\nu\rangle_l = \sum_J w(IJ)\left\langle \mu \left| \left[\mathbf{T}_{JI} \sum_{l'} \sum_{m'} \mathbf{M}_{l'}^{m'}(J) \right]_l^m \right| \nu \right\rangle, \qquad (5)$$

where

$$\left[\mathbf{T}_{JI} \sum_{l'} \sum_{m'} \mathbf{M}_{l'}^{m'}(J) \right]_l^m$$

is the (lm) component in I resulting in the multipole operators defined at center J. From a technical point of view, all calculations in this study were performed with the following parameters: the maximal order of the multipolar expansion is 6, all nuclei are chosen as center for the multipolar expansion, the relative dielectric constant inside the cavity is equal to 1 (vacuum), and the cavity has the shape of the molecule following the algorithm of J. L. Pascual-Ahuir (GEPOL93). For similar cavities and calculation level, both the PCM and NCM should provide exactly the same electrostatic contribution to the free enthalpy of solvation [24]. Even if cavitation and dispersion [25, 26] terms can also be evaluated in NCM formalism (i.e., using the Pierrotti [13–15] model for cavitation), these calculations are rarely performed. The reason is that these terms can only be grossly evaluated and often almost cancel each other out.

The choice of shape and dimension for the solute is one of the most delicate steps in defining a continuum solvation model. For both models, the solute cavity is built on interlocking spheres, usually centered on atoms or atomic groups. Although almost identical, the generation of the cavities in PCM and NCM slightly differs [27]. In the framework of PCM, different cavities are considered to calculate the various components to the solvation energy. For the electrostatic contribution, the de-

fault surface is solvent excluding surface (SES) [28]. The surface is built from spheres, centered on atoms, on which solvent spheres with a defined radius are rolled. Many possible choices for the atomic radii have been proposed. One of the most refined treatments uses optimized radii calibrated on the solvation energies of a representative set of solutes [29, 30]. In NCM, the standard criterion used to compute the energy of solvation is based on Onsager works, the purpose of which is to use the average volume occupied by a molecule [31].

Practically, in the present work we consider for the NCM formalism, a multicentric expansion of the multipolar development with molecular-shaped (S_{vdW}) [32] cavities represented as a superposition of overlapping nuclear centered spheres with radii equal to Bondi values [33] scaled by a factor of 1.3084 (B. Teryn, personal communication). This choice is made to obtain a cavity volume consistent with Onsager's theory for polar liquids. In the case of PCM, the sphere radii used are of the UAO type scaled by a factor of 1.2. PCM and NCM calculations have been performed respectively with the standard Gaussian 03 package [28] and the modified Gaussian 03 package (SCRFPAC) developed by Rinaldi and Pappalardo [34]. All calculations follow the methodological procedure:

1. Optimization of the ground-state geometry at the B3LYP/6-311G(2*d*,2*p*) level of theory with a tight (SCF convergence at 10^{-11}) threshold: After the minimization process, we perform a vibrational analysis.
2. Determination of the vertical electronic excitation energies using the TD-DFT framework: In the case of coumarin, it has been shown that the 6-311+G(2*d*,2*p*) [35] is an adequate basis set. However, for NCM calculations, the presence of diffuse functions leads to a SCF cycle divergence caused by the extension of the electronic cloud outside the cavity boundary. Nevertheless, this problem is definitively solved by slightly reducing the initial basis to 6-311G(2*d*,2*p*). Because we study electronic spectra in the present work, we have selected the nonequilibrium PCM and NCM solutions [5]. Indeed, the absorption presents a short characteristic time. Therefore, only the solvent electronic distribution can adapt to the new (excited) electronic structure of the solute, while molecular motions of the solvent are frozen during the process. If full relaxation of the solvent is allowed, one obtains the so-called equilibrium PCM solutions [5].

DFT orbitals are obtained by solving the Kohn–Sham equation, involving exchange and correlation (XC) terms. Numerous XC functionals have been developed, and an adequate choice is crucial to obtain reliable results. In a first group, one finds the local density approximation (LDA) functionals. In this scheme, a potential due to a spherical and uniform distribution of the allocated density charge to each electron: this approximation is often inappropriate for studying the excitation spectra [35]. In a second group, one finds the gradient corrected functionals [generalized gradient approximation (GGA)], for example, BLYP [36, 37] (Becke's exchange and Lee, Yang, Parr (LYP) correlation) and Perdew–Burke–Erzenrhof (PBE) [38, 39]. In this scheme, the exchange-correlation potential is a function of both the density and its gradient. Compared with LDAs, pure GGA functionals provide superior results, although they are unable to deliver correct values for most of the dye properties (geometry, UV and UV/VIS spectrum). In a third group, one finds hybrid functionals that are currently favored by the computational chemists, and that include a fraction of exact exchange (i.e., Hartree–Fock). Typically, the so-called three-parameter hybrids are built as follows:

$$E^{XC} = E^{LDA\text{-}XC} + \beta_1(E^{HF} - E^{LDA\text{-}XC}) + \beta_2\Delta E^{GGA\text{-}X} + \beta_3\Delta E^{GGA\text{-}C}, \quad (6)$$

where the GGA corrections on the exchange and correlation energies explicitly appear. The β_i parameters are often optimized with a method of least-squares fitting on experimental data (e.g., atomization enthalpies, ionization potentials). In this work, we used O3LYP [40] ($\beta_1 = 0.1161$, $\beta_2 = 0.9262$, $\beta_3 = 0.8133$), B3LYP [41, 42] ($\beta_1 = 0.20$, $\beta_2 = 0.72$, $\beta_3 = 0.83$). PBE0 [43, 44] is built on the ACM1 approach, in which $\beta_4 = 0.25$:

$$E^{XC} = E^{HF} + (1 - \beta_4)E^{GGA\text{-}X} + E^{GGA\text{-}C}. \quad (7)$$

3. Results

3.1. SCRF FORMALISM EFFECTS ON VIBRATIONAL SPECTRA

In this section, the anharmonicity correction to the fundamental wave numbers is carried out

by scaling the calculated harmonic frequencies. Andersson and Udval [45] demonstrated in recent work that, at the B3LYP framework, this value is quite sensitive to the selected basis set. Moreover, they show that the theoretical values calculated with 6-311+G(*d*,*p*) have to be corrected by a factor of 0.9679. Since this basis set is close to the one we used, we have chosen to scale our wave numbers by the same amount. The PCM–NCM (standard versions) and experimental coumarin C═O stretching mode wave number ($\upsilon_{C=O}$) and intensities ($I_{C=O}$) dependence with the surrounding dielectric constant (ε_r) are firstly studied. The $I_{C=O}$ and $\upsilon_{C=O}$ evolutions as a function of ε_r are drawn in Figure 2, and the values are given in Table I.1 (see Supplementary Material). Figure 2 shows a nice correlation among the three evolutions for which we can observe a saturation of both $I_{C=O}$ and $\upsilon_{C=O}$ for a $\varepsilon_r^{Solvent}$ superior to 5. Moreover, PCM wave numbers are systematically lower than NCM ones, whereas the IR intensities are larger with the former one. This PCM–NCM discrepancy can be explained by the different cavities used to compute the solute–solvent interactions energy; consequently, it is obvious that the solute polarized wave functions are not similar. In Figure 2 one clearly sees that the PCM–NCM $I_{C=O}$ and $\upsilon_{C=O}$ differences are lower for smaller ε_r, due to the weak electrostatic interactions. To ease the comparison, one can choose an identical type of solute cavity for both models. Because it is a common option to PCM and NCM, we go to the van der Waals (vdW) type of surface with Bondi-type atomic radii of 1.70, 1.52, and 1.20 Å for C, O, and H, respectively. On the other side, from the starting vdW values of coumarin atomic radii, a scan of the cavity size has been performed with scale factors α (atomic sphere growth factor) of 1.1, 1.2, 1.3, 1.4, 1.5, 3.0, and 5.0. Table I.2 (see Supplementary Material) provides the $\upsilon_{C=O}$ dependence to solute cavity size which is drawn in Figure 3 for calculations performed in benzene and in ethanol. Note that because of memory storage limitations, calculations of $\upsilon_{C=O}$ for α values superior to 3.0 are made difficult in the PCM framework. As depicted in Figure 3, since the electrostatic contribution to the solvation energy goes to zero for infinite value of α, the NCM $\upsilon_{C=O}$ limit is calculated to be 1758 cm^{-1} which is indeed the value for the isolated system (molecule in gas phase). In the case of PCM, the extrapolated value for α going to infinity does not correspond to the gas-phase calculation. In other words, for a similar value of cavity volume (V), we get two different values of $\upsilon_{C=O}$. Moreover,

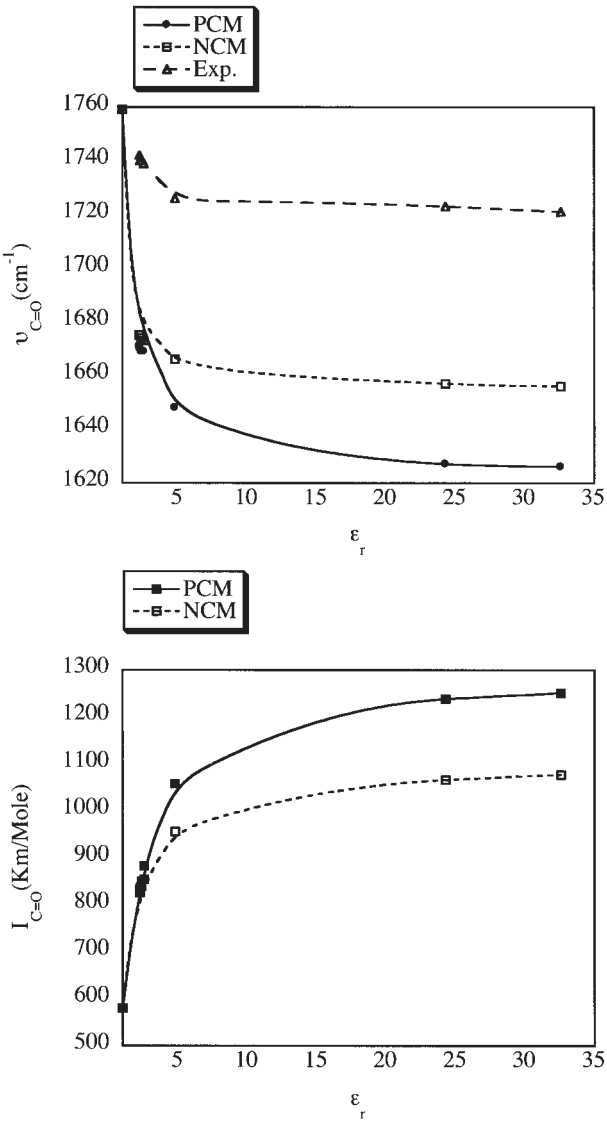

FIGURE 2. Comparison between PCM, NCM, and experimental C═O stretching wave number (in cm^{-1}) and intensity (in $km \cdot mol^{-1}$) of coumarin in various solvent of dielectric constant ε_r.

Figure 3 shows that, in the case of coumarin in ethanol, only NCM model permits a calibration adjustment of the cavity volume, to minimize the theory–experiment discrepancies. The optimal agreement for $\upsilon_{C=O}$ [experimental $\upsilon_{C=O}$ values 1723 cm^{-1}] is reached in EtOH for a cavity volume of ~270 $Å^3$ (cavity surface of ~230 $Å^2$), which corresponds to a α value close to 1.5. Using the NOCAV, NODIS, and NOREP options in the PCM formalism (which avoid the calculations of cavitation, dispersion, and repulsion energies, respec-

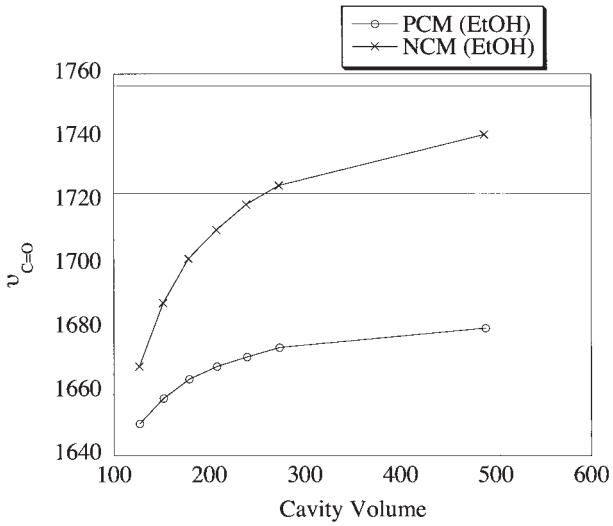

FIGURE 3. Asymptotic evolution of C═O stretching wave number (in cm^{-1}) of coumarin with the volume cavity size of the solute (expressed in $Å^3$). IR spectra are obtained at the NCM-PCM(EtOH)/B3LYP/6-311G(2*d*,2*p*) level. The limit at 1758 cm^{-1} corresponds to the theoretical value of the stretching wave number in vacuum and the second line corresponds to the experimental value.

tively) leads identical values of $\upsilon_{C=O}$ than those listed in Table I.2. Obviously the possibility of non-electrostatic terms which influence the vibrational treatment has to be ruled out.

The main origin of the PCM–NCM is attributed to the fact that the PCM formalism does not take into account the whole set of options: i.e., in our case, the Bondi-type atomic radii option is not applied during the entire process of geometry optimization. Table I.3 shows the PCM–NCM evolution with the scaling factor α ($\alpha = \infty$ corresponds to the solute in gas phase) of several ground-state properties of the trifluoromethane in tetrachloromethane, the target properties are: (i) the dipolar moment μ (in Debye), (ii) the cavity surface (S in $Å^2$) and volume (V in $Å^3$), (iii) the C—H and C—F bond length (d in Å), (iv) the electrostatic energie of solvation (in kcal · mol^{-1}), and (v) unscaled IR frequencies (expressed in cm^{-1}) and their corresponding symmetry label. From Table I.3 (Supplementary Material), one can see that, if close cavity sizes are preserved during the geometry optimizations and the vibrational calculations, both SCRF models provide quasi-identical IR spectra: as expected, the major discrepancies occur for the vibrational modes of highest energies (A_1''' and E‴ modes of vibration). The slight divergences between the PCM and NCM IR spectra can be related to the fact that the ground-state electrostatic energies also differ. There are several reasons why the electrostatic energies differ even when one uses the same cavity definitions [24]. Chief among these may be the way in which the solute charge is represented. Indeed, the PCM calculations use the full solute wave function, whereas the NCM model uses a distributed multipole expansion. A second difference is the outlying charge error treatment. The NCM treats all solute charge effects arising from multipoles within the cavity; hence outlying charge error is not manifest. As shown in Table I.3 (Supplementary Material), this effect is particularly huge when (i) small solute cavity size are used (for small value of α) for which we register the largest NCM–PCM discrepancies in E_{elect} calculations, and (ii) high dielectric solvent is used. Indeed, as shown in Table I.4 (Supplementary Material), the NCM–PCM differences for the A_1''' and E‴ modes of vibration is sensitively higher for α values inferior to 1.5: 40 cm^{-1} at maximum (α = 1.0), corresponding to a difference in solvation electrostatic energies of 1.6 kcal · mol^{-1}. Compared with calculations in weaker dielectrical surrounding (see Table I.3, Supplementary Material), the NCM–PCM electrostatic energies difference is inferior to 0.20 kcal · mol^{-1} in average [from α: 1.0 to 3.0] suggesting that both models are equivalent when identical solute cavity sizes are used. Moreover, D. Rinaldi et al. [21] show that for a identical solute cavity volume, the equivalence NCM–PCM remains useful for reasonable dielectrical surroundings, i.e., the solvent used is acetonitrile (ε_r of 36.6).

It is of interest to check whether the optimal scale factor value is identical (or included in a same interval) for the whole IR spectrum: the α dependence of the coumarin IR spectra calculated in benzene is depicted in Figure 4, which shows that only the stretching mode involving the O—C═O group (band of a maximal intensity) is significantly affected by the change of the cavity size (+61 cm^{-1} shift), the rest of the spectrum remaining almost untouched: The C—C and C—H bending (in plane: 600–700 cm^{-1}, out of plane: 1200–1500 cm^{-1}), stretching (C—C: 3000–3200 cm^{-1}, C—H: 1500 cm^{-1}), bands are not affected by the α variation, whereas the O—C═O bending band is weakly modified (+3 cm^{-1}). To further analyze the frequency modification, one can isolate two factors that are susceptible to modify the PCM and NCM sensitivity to α variation: (i) the solute polarity (in the coumarin case, only the stretching mode of the more polar group is affected by the change of cavity

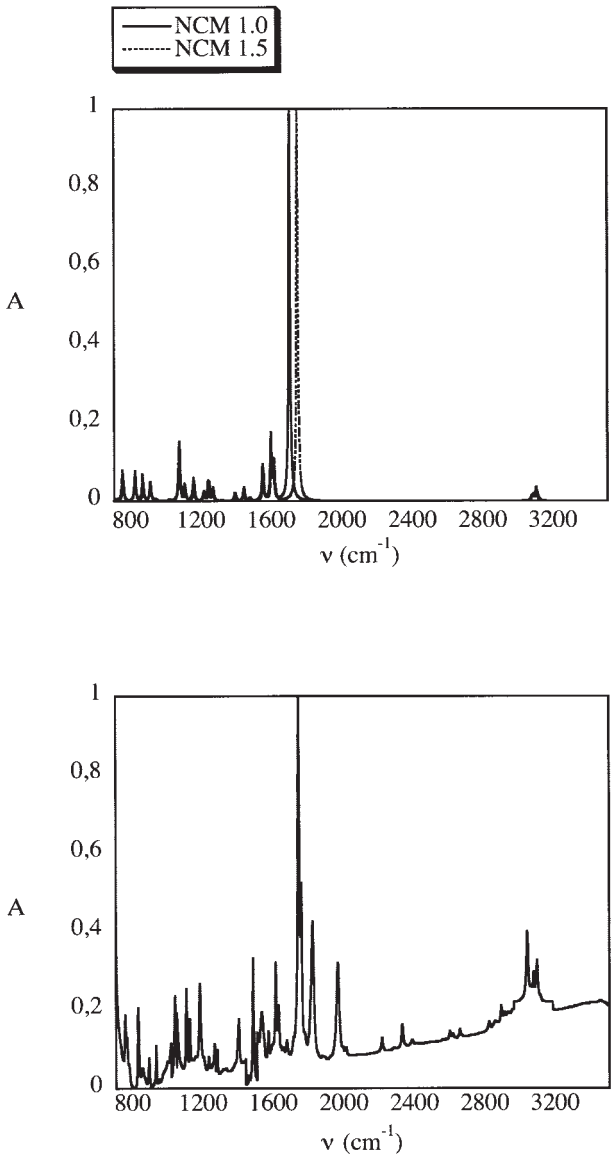

FIGURE 4. Comparison between theoretical IR spectra (up) and experimental spectrum of coumarin in benzene solution (down). The evolution of the benzene-phase IR spectrum with α (varying from 1.0 to 1.5) is also provided. All geometries are obtained at the NCM(C_6H_6)/B3LYP/6-311G(2*d*,2*p*) level. The experimental spectrum has been taken with a Perkin-Elmer spectrum RX IFT-IR system.

size), and (ii) the solvent polarity [as shown in Table I.2 (Supplementary Material) the coumarin $\upsilon_{C=O}$ variation range is larger in EtOH than in C_6H_6].

3.1.1. Solute Polarity Effects

Since PCM and NCM formalisms provide nearly identical results in weak or reasonable dielectrical surroundings when a common solute cavity size is used for the geometry optimizations as well as for vibrational calculations, the results gathered in Tables I and II are common to the two SCRF models [46]. For the set of solutes listed in these tables, only the bands of maximal intensity are sensitive to the change of α. As an example, for CH_3F, CF_3H, and CF_4, we calculate a variation range [$\Delta\upsilon = \upsilon(\alpha = 3.0) - \upsilon(\alpha = 1.0)$] for the C—F bending modes (for which the relative intensities are close to zero) of only $+3$ cm^{-1} on average. These results are in perfect agreement with the coumarin IR spectrum behavior depicted in Figure 4, for which the O—C═O bending mode variation is of $+6$ cm^{-1} (it represents only 9% of variation range obtained for the C═O stretching mode frequency) for α going from 1.0 to 1.5.

Table I lists the stretching modes, which are deeply affected by the cavity size change. In Table I, the wave number evolution, with respect to the scaling factor, is evaluated in CCl_4 for a set of 8 solutes of various polarity. The starting Bondi-type atomic radii (in Å) are of 1.47 for F, 1.75 for Cl, 1.55 for N, and 1.85 for the Br atom. From the wave number variations, one can deduce the effects induced by the change of the solute polarity (indicated in Tables I and II by the relative dielectric constant $\varepsilon_r^{\text{solute}}$, as well as the gas-phase dipole moment $\mu_{\text{gas}}^{\text{solute}}$ values) on the IR spectra. It turns out that there is no direct correlation between $\mu_{\text{gas}}^{\text{solute}}$ and $\varepsilon_r^{\text{solute}}$, and the variation of the stretching wave number value with α. For example, the frequencies shift of the C—H and C—F stretching mode in methane and fluoromethane molecules are of -4 cm^{-1} and $+32$ cm^{-1}, respectively, although both molecules have no permanent dipole moment and very close dielectric constants. In contrast, as shown in Table I, the frequency variation range of the C—F stretching mode of CH_3F is three orders of magnitude weaker than in CF_3H, in spite of the fact that $\varepsilon_r^{CH_3F}$ is higher than $\varepsilon_r^{CF_3H}$ by a factor 10. One can also express the polarity of the bond by using the partial atomic charges q (computed within the Mulliken partitioning in the gas phase). Indeed, a relation between the atomic charges and the wave number shifts when α increases does exist. For the CH_3F, CF_3H, and CF_4 set of molecules, the Mulliken atomic charge borne by the F atom is -0.36, -0.28, and -0.25 e, respectively, whereas the frequency shifts are of $+7$, $+20$, and $+32$ cm^{-1}. This statement also holds for the largest C_6H_5F molecule, for which we calculate a q_F value of -0.30 e and a variation range of $+11$ cm^{-1}. We also consider the difference

TABLE I

Stretching wave number (in cm^{-1}) evolution υ with the scale factor α (from 1.0 to 3.0) of selected 8 solutes in CCl_4 solvent.*

Solutes	ε_r^{solute} [45]	μ_{gas}^{solute}	Vibrational mode	Δq	υ 1.0	1.1	1.2	1.3	1.4	1.5	2.0	3.0	$\Delta\upsilon$
CH_4	1.68	0	Stretching C—H	−0.35	2937	2338	2939	2939	2940	2940	2940	2940	+3
CH_3Br	9.71	1.917	Stretching C—Br	−0.13	547	553	557	558	560	561	564	566	+19
CBr_4	—	0	Stretching C—Br	−0.75	594	598	601	603	603	604	606	607	+13
CH_3Cl	10.00	2.0376	Stretching C—Cl	0.10	653	662	667	671	673	674	678	680	+27
CCl_4	2.23	0	Stretching C—Cl	0.04	686	692	695	697	698	699	703	705	+18
CH_3F	51.00	1.7476	Stretching C—F	0.61	990	999	1005	1010	1012	1014	1020	1023	+33
CF_3H	5.20	1.524	Stretching C—F	1.11	1088	1091	1092	1093	1094	1095	1097	1098	+10
			Stretching C—H	0.84	3071	3062	3054	3048	3043	3040	3033	3031	−40
CF_4	1.69	0	Stretching C—F	1.24	1195	1201	1206	1209	1212	1213	1219	1221	+26

* For all the studied compounds, the wave numbers reported in this Table correspond to stretching modes of maximum intensity. For each compound, the variation range $\Delta\upsilon$ is related to the solute dielectric constant ε_r^{solute}, the solute gas-phase dipole moment μ_{gas}^{solute} (in Debye), and the charge difference Δq (in e) of the bond involved in the vibrational mode.

of charges (Δq) carried by each bonded atoms implied in the stretching mode, i.e., the C and F atoms in this case. This difference of charges is 0.61, 1.11, and 1.24e for CH_3F, CF_3H, and CF_4 solutes, respectively, showing a monotonic but not linear behavior. Obviously, the larger the Δq, the larger the variation range, permitting the calibration of the solute cavity size. In the case of bromomethane derivatives, it is the reverse: the larger the Δq, the weaker the variation range. This can be explained by the fact that, in the case of bromo-derivatives, the positive charge of the polarized C—Br bond is carried by the Br atom(s), whereas for the fluoro-derivatives, the electronic density of the C—F bond is located on the F atom(s).

3.1.2. Solvent Polarity Effects

Table II shows the impact of the solvent's relative dielectric constant ($\varepsilon_r^{solvent}$) on υ variation. It turns out that the wave number sensitivity to the change of cavity size is greater for large $\varepsilon_r^{solvent}$. For the chloro- and fluorobenzene, for which IR spectra are calculated in a weak dielectrical environment (see Table II), the experimental values are never reached, whatever the value of α. One can also note that, in general, for both SCRF formalisms, a decrease of $\varepsilon_r^{solvent}$ leads to an increase in the stretching mode wave number, which is in general too large, and the experimental value is overshot. Since for α values inferior to 1.0, imaginary wave numbers appear, and taking into account the fact that PCM calculations become difficult (because of memory storage limitation) for α values superior to 3.0, it is then more difficult to calibrate the PCM solute cavity size for calculation in solvents with a weak dielectric constant.

On the other side, note that, for molecules presenting large ε_r (i.e., nitromethane, -ethane, and -benzene), a calibration is possible whatever the $\varepsilon_r^{solvent}$ value and the solute size (described by $V_{\alpha=1.0}^{cav}$ in Table II) and the optimal α tends to a common value (of 1.5). In the nitrobenzene case, for which we calculate the largest $V_{\alpha=1.0}^{cav}$ (105 $Å^3$ compared with 51 and 68 $Å^3$ for nitromethane and nitroethane, respectively) value and the lowest variation range of N═O stretching (+24 cm^{-1} in CCl_4), one can see that the optimal α is $\varepsilon_r^{solvent}$-independent and can be estimated at 1.5 for a calibration performed in CCl_4 or in pure liquid phase. It is important to underline that, in the coumarin case (for which we get a $V_{\alpha=1.0}^{cav}$ of 127 $Å^3$ and a 4.67 D dipole moment, i.e., very close to $C_6H_5NO_2$ one), we also get a very close $\varepsilon_r^{solvent}$-independent value of α (see Tables I.1 and I.2, Supplementary Material).

3.2. SCRF FORMALISM EFFECTS ON UV SPECTRA

We have used a training set of five molecular systems directly deriving from coumarin, for which we used the standard substitution position labeling (5-Me; 6,7-diOH; 7,8-diOH; 6-Cl; and 6-NH_2 in Fig.

TABLE II

Stretching wave number (in cm^{-1}) evolution with the scale factor α (from 1.0 to 3.0).*

Solutes	Solvents	ε_r^{solute} [44]	$\varepsilon_r^{solvent}$ [44]	μ_{gas}^{solute}	$V_{a=1.0}^{cav}$	Vibrational mode	α 1.0	1.1	1.2	1.3	1.4	1.5	2.0	3.0	$\nabla\nu$	Exp. [46]
CH_3NO_2	CCl_4	38.2	2.2	3.38	51	Stretching C—N	637	637	637	637	637	637	637	637	0	666
	CH_3NO_2		38.2				638	638	638	638	637	637	637	637	−1	667
	CCl_4					Stretching N═O	1551	1556	1561	1566	1569	1571	1577	1580	+29	1565
	CH_3NO_2						1505	1525	1538	1547	1553	1558	1571	1580	+75	1562
$C_2H_5NO_2$	CCl_4	29.1	2.2	3.50	68	Stretching C—N	853	854	854	854	854	854	855	855	+2	874
	$C_2H_5NO_2$[a]		29.1				854	854	854	854	854	854	854	854	0	876
	CCl_4					Stretching N═O	1543	1551	1556	1561	1564	1566	1571	1575	+32	1557
	$C_2H_5NO_2$						1506	1524	1535	1543	1549	1554	1566	1573	+67	1556
C_6H_6	C_6H_6	2.3	2.3	0	84	Stretching C—H	3066	3066	3066	3066	3065	3065	3065	3065	−1	3036
C_6H_5F	CCl_4	5.5	2.2	1.41	88	Stretching C—F	1237	1241	1243	1245	1247	1248	1251	1253	+16	1223
	C_6H_5F[b]		5.5				1187	1192	1198	1200	1203	1205	1210	1213	+26	1220
C_6H_5Cl	CCl_4	5.7	2.2	1.94	98	Stretching C—Cl	1090	1092	1094	1095	1096	1097	1098	1099	+9	1085
	C_6H_5Cl		5.7		98		1051	1054	1056	1057	1059	1060	1062	1064	+13	1083
$C_6H_5NO_2$	CCl_4	35.6	2.2	4.39	105	Stretching C—N	1327	1329	1330	1330	1331	1331	1332	1333	+6	1349
	$C_6H_5NO_2$[c]		35.6				1315	1318	1321	1323	1324	1326	1330	1333	+18	1347
	CCl_4					Stretching N═O	1515	1521	1525	1527	1530	1532	1536	1539	+24	1531
	$C_6H_5NO_2$						1489	1500	1508	1514	1518	1521	1530	1537	+48	1521

* For each solute, the theoretical results are compared with experiment. In this table, the variation $\Delta\nu$ is related to the solute dielectric constant value ε_r^{solute}, the solute gas-phase dipolar moment μ_{gas}^{solute} (in Debye), and the solute cavity size $V_{a=1.0}^{cav}$ (in Å^3). For all the studied compounds, the wave numbers reported in this Table correspond to stretching modes of maximum intensity.

[a] Nitroethane as nitromethane, except for EPS = 29.11 and VMOL = 86.65 Å^3.

[b] Fluorobenzene as chlorobenzene, except for EPS = 5.47 and VMOL = 132.01 Å^3.

[c] Nitrobenzene as chlorobenzene, except for EPS = 35.60 and VMOL = 152.77 Å^3.

TABLE III

Solvation model effect on the calculated λ_{max}.*

	Gas UV			Gas geometry PCM(EtOH) UV			NCM(EtOH) UV		
Substituents	O3LYP	B3LYP	PBE0	O3LYP	B3LYP	PBE0	O3LYP	B3LYP	PBE0
5-Me	313	304	296	314	304	296	315	303	295
6-Cl	324	313	305	319	309	301	320	308	300
7,8-diOH	325	301	294	351	331	320	346	326	314
6,7-diOH	341	329	320	349	336	326	345	330	321
6-NH_2	380	362	351	402	381	367	398	373	360
	Gas UV			PCM (EtOH) geometry PCM(EtOH) UV			NCM(EtOH) UV		
Substituents	O3LYP	B3LYP	PBE0	O3LYP	B3LYP	PBE0	O3LYP	B3LYP	PBE0
5-Me	313	304	296	314	304	296	315	304	296
6-Cl	319	309	301	319	309	301	321	309	300
7,8-diOH	339	321	309	351	332	320	346	326	315
6,7-diOH	341	329	320	349	336	326	347	333	323
6-NH_2	380	363	351	403	381	367	402	378	364
	Gas UV			NCM (EtOH) geometry PCM(EtOH) UV			NCM(EtOH) UV		
Substituents	O3LYP	B3LYP	PBE0	O3LYP	B3LYP	PBE0	O3LYP	B3LYP	PBE0
5-Me	313	305	297	314	305	297	315	304	295
6-Cl	324	314	305	320	310	302	321	309	300
7,8-diOH	337	320	309	351	332	321	346	325	314
6,7-diOH	342	330	321	350	337	328	346	331	322
6-NH_2	382	364	352	406	381	370	401	376	363

* All geometries are obtained at the B3LYP/6-311G(2*d*,2*p*) level. UV spectra are always obtained at the TD-DFT/6-311G(2*d*,2*p*) level.

1). The experimental maximum absorption wavelength (λ_{max}) in ethanol is known for each of these molecules: 315, 354, 335, 321, and 370 nm, respectively [47]. The theoretical λ_{max} reported in the following corresponds to the first singlet excited state for which a dipole-allowed transition (i.e., nonzero oscillator strength) from the ground state is found.

In the theoretical approach, one can formally split the solvent effects on the electronic spectrum into two components: (i) a modification of the ground-state geometry (*indirect* component) and (ii) a perturbation of the UV spectra (*direct* component). The relative weight of the two contributions is shown in Table III, in which we provide the λ_{max} calculated with the standard versions of SCRF models. It turns out that the modification in the ground-state geometry due to the change of solvation model has an slight impact on λ_{max} (average difference of ~ -4 nm). In contrast, the change on the excitation spectrum is not of constant magnitude, and one can split the five studied compounds into two groups: (i) the 5-Me and 6-Cl derivatives for which λ_{max} are identical, whatever the SCRF formalism used for the TD-DFT calculations; and (ii) the more polar 7,8-diOH, 6,7-diOH, and the 6-NH_2 for which λ_{max} are affected by this change ($\sim$6 nm on average). Obviously, the difference is independent of the functional used for TD calculations and seems to be more significant for most polar solutes 7,8-diOH, 6,7-diOH, and the 6-NH_2-coumarin. Moreover, since PCM solute–solvent nonelectrostatic interactions are not taken into account in the TD calculations, the discrepancies might origin in the fact that the standard cavities used in each model are not identical. More precisely, NCM cavities are systematically larger than the PCM ones (e.g., for 6-Cl derivative, NCM pro-

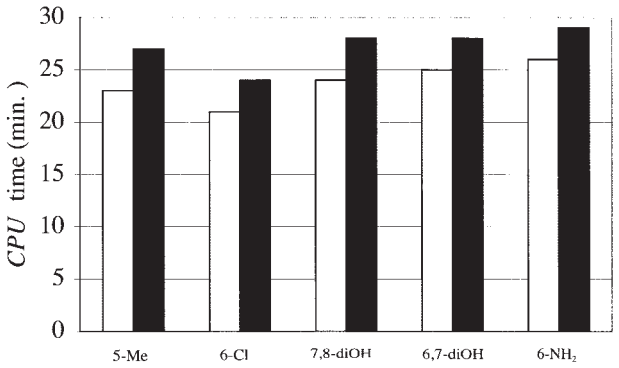

FIGURE 5. Comparison between NCM (□) and PCM (■) required CPU times (minutes) for TD-DFT calculations. All calculations have been performed in the UV spectra are always obtained at the PCM(EtOH)-TD(B3LYP)/6-311G(2*d*,2*p*) level of theory.

vide a 236 Å^3 cavity surface whereas PCM cavity is of 193 Å^3); this change in cavity size affecting the more polar solutes. Nevertheless, the average difference between λ_{max}^{NCM} and λ_{max}^{PCM} is slight; let us suggest that the choice of cavity size has a minor impact on the UV treatment.

In recent work, Rinaldi et al. [21] show that the required time for the geometry optimization starting from the gas phase structure as well as for vibrational treatments is in general quasi-equivalent for both SCRF formalisms used [21]. In contrast, as depicted in Figure 5 (the data are listed in Table IV), for TD-DFT calculations, the required CPU time is slightly sensitive to the choice of the SCRF model. As shown in Figure 5, NCM calculations time is reduced by 3 min (on average), which corresponds to a saving of 13% of the total required CPU time.

4. Conclusions and Outlook

We have reported a comparison of the liquid-phase IR and UV spectra as a measure of the response of the solute to the reaction field of several solvents. Both properties (resulting from PCM and NCM approaches) have been compared with, and confronted to, experimental data. In this context, the solute cavity size is shown to be an essential factor for these calculations and a scale factor (α), by which the atomic radii are multiplied, is introduced to permit fitting of the theoretical results. Two factors which modify the PCM and NCM sensitivity to α have been highlighted: the solute polarity and the solvent polarity. The results point out a more marked sensitivity of the IR spectra to these factors. More precisely, it has been established that a large solute polarity is a necessary condition to permit calibration of the solute cavity size. A direct consequence is that, for any solute, only the vibrational modes implying a (or more than one) polar groupment of the molecule is liable to be calibrated. Practically, as shown for coumarin, a calibration of the IR spectrum is conceivable for the only vibrational modes of maximal intensity.

Considering the UV spectra of coumarin derivatives, a comparison of λ_{max} that results from both standard SCRF formalisms shows that NCM and PCM provide quasi-identical values of λ_{max}, independently of the chosen cavities, although the former can be carried out at significantly lower CPU costs. As an outlook, we are actually testing the reliability of the NCM model in the evaluation of coumarin derivatives UV spectra for which an efficient an adaptable theoretical scheme has been designed [35].

ACKNOWLEDGMENTS

J. P. acknowledges the FRIA (Belgian Fonds pour la formation à la Recherche dans L'Industrie et dans l'Agriculture) for his PhD grant. D. J. and E. A. P. thank the Belgian National Fund for their respective Research Associate positions. The calculations have been performed in part at the Interuniversity Scientific Computing Facility (ISCF), installed at the Facultés Universitaires Notre-Dame de la Paix (Namur, Belgium).

TABLE IV

Required NCM–PCM CPU times for TD calculations (minutes).*

Compounds	CPU time	
	NCM	PCM
5-Me	23	27
6-Cl	21	24
7,8-diOH	24	28
6,7-diOH	25	28
6-NH_2	26	29

* UV spectra are always obtained at the TD-B3LYP/6-311G(2*d*,2*p*) level.

[a] Calculations performed with IBM RS6000 workstation.

References

1. Cramer, C. J.; Truhlar, D. G. Chem Rev 1999, 99, 2161.
2. Tomasi, J.; Persico, M. Chem Rev 1994, 94, 2027.
3. Tomasi, J.; Mennucci, B.; Cammi, R. Chem Rev 2005, 105, 2999.
4. Hirsh, J.; Dalen, J. E.; Anderson, D. R.; Poller, L.; Bussey, H.; Ansell, J.; Deykin, D. Chest 2001, 119, 8S.
5. Cossi, M.; Barone, V. J Chem Phys 2001, 115, 4708.
6. Cancès, M. T.; Mennucci, V.; Tomasi, J. J Chem Phys 1997, 107, 3032.
7. Mennucci, B.; Cammi, R.; Tomasi, J. J Chem Phys 1999, 110, 6858.
8. Cossi, M.; Barone, V.; Mennucci, V.; Tomasi, J. Chem Phys Lett 1998, 286, 253.
9. Mennucci, B.; Tomasi, J. J Chem Phys 1997, 106, 5151.
10. Mennucci, B.; Cancès, E.; Tomasi, J. J Phys Chem B 1997, 101, 10506.
11. Tomasi, J.; Mennucci, B.; Cancès, E. J Mol Struct (Theochem) 1999, 464, 211.
12. McWeeny, R. Methods of Molecular Quantum Mechanics; Academic Press: London, UK, 1992.
13. Pierotti, R. A. J Phys Chem 1963, 67, 1840.
14. Pierotti, R. A. J Phys Chem 1965, 69, 281.
15. Pierotti, R. A. Chem Rev 1976, 76, 712.
16. Rinaldi, D.; Rivail, J.-L. Theor Chim Acta 1973, 32, 57.
17. Rivail, J.-L.; Rinaldi, D. Chem Phys 1976, 18, 233.
18. Rinaldi, D.; Ruiz-Lopez, M. F.; Rivail, J.-L. J Chem Phys 1983, 78, 834.
19. Dillet, V.; Rinaldi, D.; Rivail, J.-L. J Phys Chem 1994, 98, 5034.
20. Rinaldi, D.; Bouchy, A.; Rivail, J.-L.; Dillet, V. J Chem Phys 2004, 120, 2343.
21. Rinaldi, D.; Bouchy, A.; Rivail, J.-L. Theor Chem Acc 2006, 116, 664.
22. Stone, A. J. The Theory of Intermolecular Forces; Oxford University Press: Oxford, 2000.
23. Vigne-Maeder, F.; Calverie, P. J Chem Phys 1988, 88, 4934.
24. Curutchet, C.; Cramer, C. J.; Truhlar, D. G.; Ruiz-Lopez, M. F.; Orozco, M.; Luque, F. J. J Comput Chem 2003, 24, 284.
25. Rinaldi, D.; Costa, C.; Benedito, J.; Rivail, J.-L. Chem Phys Lett 1986, 125, 495.
26. Costa, C.; Benedito, J.; Rinaldi, D.; Rivail, J.-L. CR Acad Sci Ser II: Mec Phys Chim Sci Terre Univers 1984, 298, 675.
27. Floris, F. M.; Tomasi, J.; Pascual-Ahuir, J.-L. J Comput Chem 1991, 12, 1127.
28. Frisch, M. J.; Trucks, G. W.; Schlegel, H. B.; Scuseria, G. E.; Robb, M. A.; Cheeseman, J. R.; Montgomery, Jr., J. A.; Vreven, T.; Kudin, K. N.; Burant, J. C.; Millam, J. M.; Iyengar, S. S.; Tomasi, J.; Barone, V.; Mennucci, B.; Cossi, M.; Scalmani, G.; Rega, N.; Petersson, G. A.; Nakatsuji, H.; Hada, M.; Ehara, M.; Toyota, K.; Fukuda, R.; Hasegawa, J.; Ishida, M.; Nakajima, T.; Honda, Y.; Kitao, O.; Nakai, H.; Klene, M.; Li, X.; Knox, J. E.; Hratchian, H. P.; Cross, J. B.; Bakken, V.; Adamo, C.; Jaramillo, J.; Gomperts, R.; Stratmann, R. E.; Yazyev, O.; Austin, A. J.; Cammi, R.; Pomelli, C.; Ochterski, J. W.; Ayala, P. Y.; Morokuma, K.; Voth, G. A.; Salvador, P.; Dannenberg, J. J.; Zakrzewski, V. G.; Dapprich, S.; Daniels, A. D.; Strain, M. C.; Farkas, O.; Malick, D. K.; Rabuck, A. D.; Raghavachari, K.; Foresman, J. B.; Ortiz, J. V.; Cui, Q.; Baboul, A. G.; Clifford, S.; Cioslowski, J.; Stefanov, B. B.; Liu, G.; Liashenko, A.; Piskorz, P.; Komaromi, I.; Martin, R. L.; Fox, D. J.; Keith, T.; Al-Laham, M. A.; Peng, C. Y.; Nanayakkara, A.; Challacombe, M.; Gill, P. M. W.; Johnson, B.; Chen, W.; Wong, M. W.; Gonzalez, C.; Pople, J. A. Gaussian 03; Revision B 04, Gaussian: Pittsburgh, PA, 2003.
29. Rashin, A. A.; Namboodiri, K. J Phys Chem 1987, 91, 6003.
30. Stefanovic, B. V.; Truong, T. N. Chem Phys Lett 1995, 244, 65.
31. Onsager, L. J Am Chem Soc 1936, 58, 1486.
32. Dillet, V.; Rinaldi, D. Chem Phys Lett 1993, 202, 18.
33. Bondi, A. J Phys Chem 1964, 68, 441.
34. Rinaldi, D.; Pappalardo, R. R. SCRFPAC: Quantum Chemistry Program Exchange, Indiana University: Bloomington, IN, 1992; Program 622.
35. Preat, J.; Jacquemin, D.; Perpète, E. A. Chem Phys Lett 2005, 415, 20.
36. Becke, A. D. Phys Rev A 1988, 38, 3908.
37. Lee, C.; Yang, W.; Parr, R. G. Phys Rev B 1988, 37, 85.
38. Perdew, J.; Burke, K.; Ernzerhof, M. Phys Rev Lett 1997, 78, 1396.
39. Perdew, J.; Burke, K.; Ernzerhof, M. Phys Rev Lett 1996, 77, 3865.
40. Hoe, W.-M.; Cohen, A. J.; Handy, N. C. Chem Phys Lett 2001, 341, 319.
41. Becke, A. D. J Chem Phys 1993, 98, 5648.
42. Perdew, J. P. Phys Rev B 1986, 33, 8822.
43. Perdew, J. P.; Burke, K.; Wang, Y. Phys Rev B 1996, 54, 16533.
44. Adamo, C.; Barone, V. J Chem Phys 1999, 110, 6158.
45. Andersson, M. P.; Udval, P. J Phys Chem A 2005, 109, 2937.
46. Kinugasa, S.; Tanabe, K.; Tamura, T. The National Institute of Advanced Industrial Science and Technology (AIST); Bunka Women's University: Tokyo, Japan, 2006.
47. Lide, D. R. The Handbook of Chemistry and Physics; 78th ed.; CRC Press: Boca Raton, FL, 1997.